An ancient viral epidemic involving host coronavirus interacting genes more than 20,000 years ago in East Asia

Yassine Souilmi[1,2], M. Elise Lauterbur[3], Ray Tobler[1], Christian D. Huber[1], Angad S. Johar[1], David Enard[3]

[1] Australian Centre for Ancient DNA, School of Biological Sciences, University of Adelaide, Adelaide, SA 5005, Australia.

[2] National Centre for Indigenous Genomics, Australian National University, Canberra, ACT 0200, Australia.

[3] University of Arizona Department of Ecology and Evolutionary Biology, Tucson, Arizona, USA.

Summary

The current SARS-CoV-2 pandemic has emphasized the vulnerability of human populations to novel viral pressures, despite the vast array of epidemiological and biomedical tools now available. Notably, modern human genomes contain evolutionary information tracing back tens of thousands of years, which may help identify the viruses that have impacted our ancestors – pointing to which viruses have future pandemic potential. Here, we apply evolutionary analyses to human genomic datasets to recover selection events involving tens of human genes that interact with coronaviruses, including SARS-CoV-2, that likely started more than 20,000 years ago. These adaptive events were limited to the population ancestral to East Asian populations. Multiple lines of functional evidence support an ancient viral selective pressure, and East Asia is the geographical origin of several modern coronavirus epidemics. An arms race with an ancient coronavirus, or with a different virus that happened to use similar interactions as coronaviruses with human hosts, may thus have taken place in ancestral East Asian populations. By learning more about our ancient viral foes, our study highlights the promise of evolutionary information to better predict the pandemics of the future. Importantly, adaptation to ancient viral epidemics in specific human populations does not necessarily imply any difference in genetic susceptibility between different human populations, and the current evidence points toward an overwhelming impact of socioeconomic factors in the case of COVID-19.

Introduction

In the past 20 years, strains of the beta coronavirus genus (family Coronaviridae; Richman et al., 2020) have been behind three major zoonotic outbreaks with grave impacts for human populations (Ou et al., 2020). The first outbreak, commonly known as SARS-CoV (Severe Acute Respiratory Syndrome), originated in China in late 2002 and eventually spread to 30 additional counties where it infected more than 8,000 people and claimed nearly 800 lives (Hoffmann and Kamps, 2003). Four years later, MERS-CoV (Middle East respiratory syndrome coronavirus) affected >2,400 people and caused over 850 deaths, mostly in Saudi Arabia (World Health

Organization, 2019). The most recent outbreak began in late 2019 when SARS-CoV-2 – a less virulent but far more contagious strain than those behind the two previous epidemics – emerged in mainland China before spreading rapidly across the rest of the world, triggering an ongoing pandemic (COVID-19) that so far has infected 45 million people and resulted in over one million deaths worldwide (Dong et al., 2020).

The devastation caused by SARS-CoV-2 has inspired a worldwide research effort to develop new vaccines and strategies that aim to curb its impact by determining the factors that underlie its epidemiology. The resulting research has revealed that socioeconomic (e.g. access to healthcare and testing facilities or exposure at work), demographic (e.g. population density and age structure), and personal health factors all play a major role in SARS-CoV-2 epidemiology (Balogun et al., 2020; Sattar Naveed et al., 2020; Scarpone et al., 2020). Additionally, several genetic loci that mediate SARS-CoV-2 susceptibility and severity have been found in contemporary European populations (Ellinghaus et al., 2020; Roberts et al., 2020), one of which contains a genetic variant that increases SARS-CoV-2 susceptibility that likely increased in frequency in the ancestors of modern Europeans after interbreeding with Neanderthals ~40,000 years ago (Zeberg and Pääbo, 2020). This historical admixture event has led to genetic differences within and between contemporary human populations that directly impact COVID-19 epidemiology – the Neanderthal-derived variant haplotype is now carried by 8% of modern Europeans, but at lower frequencies in African populations whose ancestors did not experience this admixture event – and suggests that evolutionary analyses of human populations may help reveal these genetic differences and ultimately assist in the development of novel drugs and therapies to combat the negative impacts of SARS-CoV-2.

Throughout the evolutionary history of our species, positive natural selection has frequently targeted proteins that physically interact with viruses – e.g. those involved in immunity, or used by viruses to hijack the host cellular machinery (Barreiro et al., 2009; Enard et al., 2016; Sawyer et al., 2005). In the ~6 million years since the ancestors of humans and chimpanzees separated, selection has led to the fixation of gene variants encoding virus-interacting proteins (VIPs) at three times the rate observed for other classes of genes (Enard et al., 2016; Uricchio et al., 2019). Moreover, strong selection on VIPs has continued in human populations during the past 50,000 years, as evidenced by VIP genes being enriched for adaptive introgressed Neanderthal variants and also selective sweep signals (i.e. selection that drives a beneficial variant to substantial frequencies in a population), particularly around VIPs that interact with RNA viruses, a viral class that includes the coronaviruses (Enard and Petrov, 2018, 2020).

The accumulated evidence suggests that ancient RNA virus epidemics have occurred frequently during the history of our species; however, we currently do not know if selection has made a substantial contribution to the evolution of human genes that interact more specifically with coronaviruses.

Accordingly, here we investigate whether ancient coronavirus epidemics have driven past adaptation within and across modern human populations, by examining if selection signals are enriched within a set of 420 VIPs that interact with coronaviruses (denoted CoV-VIPs; Table S1) across 26 worldwide human populations from the 1000 Genomes Project (1000 Genomes Project Consortium, 2015). These CoV-VIPs comprise 332 SARS-CoV-2 VIPs that were recently identified by high-throughput mass spectrometry (Gordon et al., 2020) and an additional 88 proteins that were manually curated from the coronavirus literature (e.g. SARS-CoV-1, MERS, HCoV-NL63, etc; Table S1; Enard and Petrov, 2018), and form part of a larger set of 5,291 previously published VIPs (SI; Table S1) from multiple viruses known to infect humans (Enard and Petrov, 2018). Our focus upon host adaptation at VIPs is motivated by evidence indicating that these protein interactions are the central mechanism that viruses use to hijack the host cellular machinery, as shown by the strong focus of virologists on these interactions (Enard and Petrov, 2018). Accordingly, VIPs are much more likely to have functional impacts on viruses than proteins not known to interact with viruses (see SI: *Host adaptation is expected at VIPs*). Our enrichment-based approach is expected to be particularly powerful if the ancestors of one or more of the 26 modern human populations were exposed to epidemics driven by coronavirus-like viruses that resulted in selection upon multiple CoV-VIPs (see Discussion). An alternative that we cannot exclude however is that a different type of virus that happens to use similar VIPs as coronaviruses might instead create an enrichment in adaptation signals at CoV-VIPs.

Our analyses of CoV-VIPs find a strong enrichment in sweep signals in these proteins across multiple East Asian populations, which is absent from other human populations. This suggests that an ancient coronavirus epidemic (or another virus using similar VIPs) drove an adaptive response in the ancestors of East Asians, which is in agreement with the current geographic range of the major known animal reservoirs of coronaviruses (Wong et al., 2019). Further, by leveraging ancestral recombination graph approaches (Speidel et al., 2019; Stern et al., 2019) we find that amongst the putatively selected CoV-VIPs, 42 first may have come under selection around 900 generations (~25,000 years, most likely 20,000 years ago or more) ago and exhibit a coordinated adaptive response that lasted until around 200 generations (~5,000 years) ago.

By drawing upon other publicly available datasets, we show that the CoV-VIP genes are enriched for anti- and proviral effects and variants that affect COVID-19 etiology in the modern European British population (https://grasp.nhlbi.nih.gov/Covid19GWASResults.aspx). We nevertheless do not investigate in which particular direction, as we cannot expect the British population to be representative of East Asian populations in that respect. We further show that the inferred underlying causal mutations are situated near to regulatory variants active in lungs and other tissues negatively impacted by COVID-19. Taken together, these independent lines of evidence provide support for an ancient coronavirus (or another virus that was using similar interactions) epidemic that emerged more than 20,000 years ago in the ancestors of contemporary East Asian populations, whose genetic signature remains apparent in the genomes of the present-day populations now living in this region.

Results

Signatures of adaptation to an ancient epidemic

Viruses have exerted strong selective pressures on the ancestors of modern humans (Enard and Petrov, 2020; Uricchio et al., 2019). Accordingly, we use two population genetic statistical tests that are sensitive to such genetic signatures (i.e. selective sweeps) – nSL (Ferrer-Admetlla et al., 2014) and iHS (Voight et al., 2006) – and which are able to detect genomic regions impacted by strong selection across a wide range of parameters (e.g. different starting and end frequencies of the selected allele). Both statistics also have the advantage of being insensitive to background selection (Enard et al., 2014; Schrider, 2020), thereby reducing the potential impact of false positives in our analyses.

After scanning each of the 26 populations for signals of selection, we apply an enrichment test that was previously used to detect enriched selection signals in RNA VIPs in human populations (Enard and Petrov, 2020). Briefly, for each population and selection statistic, we rank all genes based on the average selection statistic score observed in genomic windows ranging from 50kb to 2Mb (Methods). Different windows sizes are used because smaller windows tend to be more sensitive to weaker sweeps, whereas larger windows tend to be more sensitive to stronger sweeps (Enard and Petrov, 2020; Methods). After ranking the gene scores, we estimate an enrichment curve (Figure 1) for gene sets ranging from the top 10 to 10,000 ranked loci (Methods). The significance of the whole enrichment curve is then calculated using a genome block-randomization approach that accounts for the genomic clustering of neighboring CoV-

139 VIPs, and provides an unbiased false positive risk for the whole enrichment curve (FPR) by re-
140 running the entire enrichment analysis pipeline on block-randomized genomes (Enard and
141 Petrov, 2020; Methods). For our control gene set, we use protein-coding genes situated at least
142 500kb from CoV-VIPs to avoid overlapping the same sweep signals. Additionally, genes in the
143 control sets are chosen to have similar characteristics as the CoV-VIPs (e.g. similar
144 recombination rates, density of coding and regulatory sequences, percentage of immune genes,
145 percentage of genes that interact with bacteria; see Methods for the complete list of factors) to
146 ensure that any detected enrichment is virus-specific rather than due to a confounding factor
147 (Enard and Petrov, 2020). Choosing controls far away and that match multiple potential
148 confounding factors has the effect of shrinking the pool of potential control genes, which can
149 affect the variance and also the representativity of this pool as a null control. The possible
150 impacts of the size of the control pool are however fully taken into account in the FPR estimated
151 with block-randomized genomes (Enard and Petrov, 2020; Methods). Finally, we also exclude
152 the possibility that functions other than viral interactions might explain our results by running a
153 Gene Ontology analysis (Gene Ontology Consortium, 2015; SI; Tables S2, S3 and Figure S1).

154 Applying this approach to each of the 26 human populations from the 1,000 genomes dataset,
155 we find a very strong enrichment of sweep signals in CoV-VIPs across all top-ranked gene set
156 sizes that is specific to the five East Asian populations (whole enrichment curve for nSL and iHS
157 combined FPR=2.10^{-4}; Figures 1 & S2; Methods). No enrichment is observed for populations
158 from other continental regions, including in neighboring South Asia (whole enrichment curve for
159 nSL and iHS combined FPR>0.05 in all cases; Figures 1 & S2). Further, no enrichment is
160 detected for VIP sets for 17 other viruses in East Asian populations (whole enrichment curve for
161 nSL and iHS separately or combined, P>0.05 in all cases; Figures S3 & S4). Taken together,
162 these results suggest that coronaviruses, or another type of viruses that used similar
163 interactions with human hosts, have driven ancient epidemics in ancient human populations that
164 are ancestral to modern East Asians. This enrichment is unlikely to have been caused by any
165 other virus represented in our set of 5,291 VIPs, but we still cannot exclude that a currently
166 unknown type of virus that happened to use similar VIPs as coronaviruses could have been
167 involved instead (Table S1). The enrichment is most substantial for the top-ranked gene sets
168 ranging between the top 10 and top 1,000 loci (Figure 1; whole enrichment curve FPR=3.10^{-6} for
169 nSL, FPR=4.10^{-3} for iHS, FPR=6.10^{-5} for iHS and nSL combined), and is particularly strong for
170 the top 200 loci in large windows (1 Mb) where a four-fold enrichment is observed for both nSL
171 and iHS statistics (pertaining to between 10 to 13 selected CoV-VIPs amongst the top 200

ranked genes; Table S4). This suggests that strong selection targeted multiple CoV-VIPs in the common ancestors of modern East Asian populations. That the selected haplotype structures are detected by both the iHS and nSL methods suggests that they are unlikely to have occurred prior to 30,000 years ago, as both nSL and iHS have little power to detect adaptive events arising before this time point in human evolution (Sabeti et al., 2006)

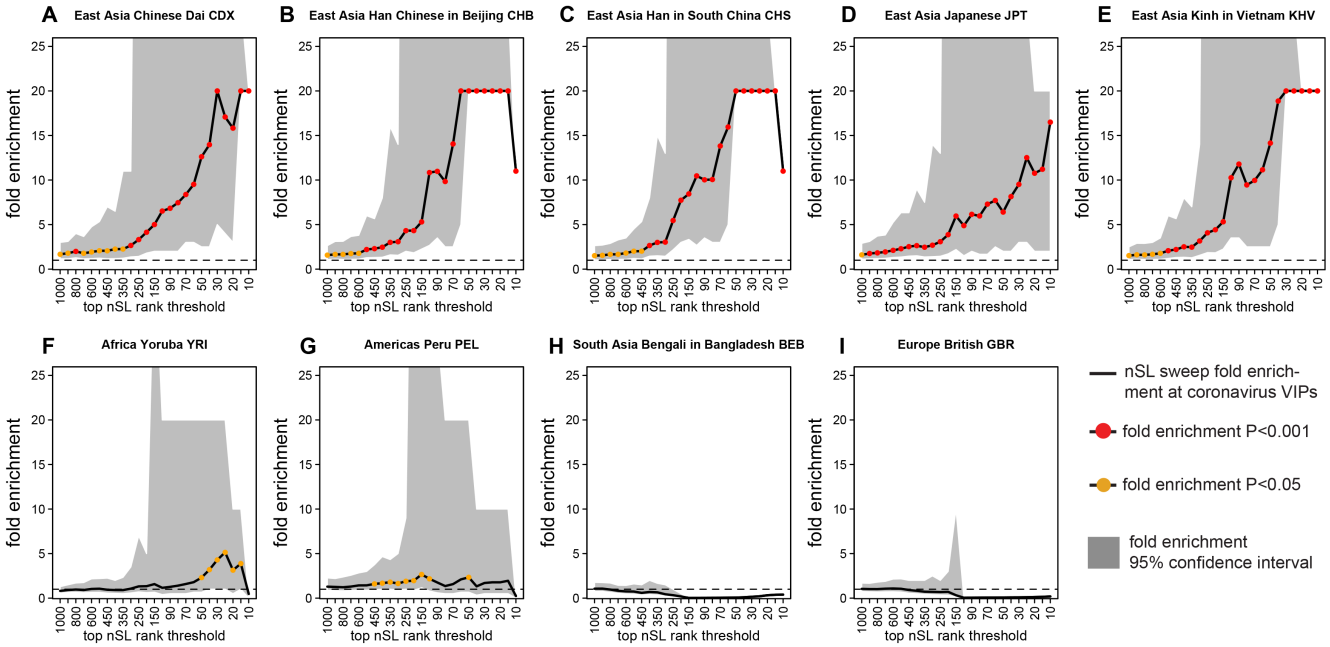

Figure 1. Coronavirus VIPs nSL ranks enrichment

A,B,C,D,E are East Asian populations, F,G,H,I are populations from other continents. The y axis represents the bootstrap test (Methods) relative fold enrichment of the number of genes in putative sweeps at CoV-VIPs, divided by the number of genes in putative sweeps at control genes matched for multiple confounding factors. The x axis represents the top rank threshold to designate putative sweeps. Black full line: average fold enrichment over 5,000 bootstrap test control sets. Fold enrichments greater than 20 are represented at 20. Grey area: 95% confidence interval of the fold enrichment over 5,000 bootstrap test control sets. The rank thresholds where the confidence interval lower or higher fold enrichment has a denominator of zero are not represented (For example, graph B, top 10 rank threshold). Lower confidence interval fold enrichments higher than 20 are represented at 20 (for example, graph B, top 30 rank threshold). Red dots: bootstrap test fold enrichment P<0.001. Orange dots: bootstrap test fold enrichment P<0.05. Note that the bootstrap test p-values are not the same as the whole curve enrichment false positive risk (FPR) estimated using block-randomized genomes on top of the bootstrap test (Methods).

195 **An ancient epidemic in the ancestors of East Asians starting more than 20,000 years ago**

196 To further test the existence of an ancient viral epidemic in the ancestors of East Asians, we use
197 a recent ancestral recombination graph (ARG)-based method, Relate (Speidel et al., 2019), to
198 infer the timing and trajectories of selected loci for the CoV-VIPs. If the selective pressure
199 responsible for the multiple independent selection events at CoV-VIPs was relatively sudden as
200 expect from a new epidemic, then these selection events should have started independently
201 around the same time. By estimating ARGs at variants distributed across the entire genome,
202 Relate can reconstruct coalescent events across time and detect genomic regions impacted by
203 positive selection, while explicitly controlling for historical variation in population demography.
204 To approximate the start time of selection, Relate estimates the first historical time point that a
205 putatively selected variant had an observable frequency unlikely to be equal to zero (Methods).
206 We use this approximation as the likely starting time of selection, although we note that this
207 method does not account for selection on standing variants that had non-zero frequencies at the
208 onset of selection (Methods). Additionally, we use the iSAFE software – which enables the
209 localization of selected mutations (Akbari et al., 2018) – along with a curated set of regulatory
210 variants (expression QTLs; eQTLs) from the eGTEx Project (2017) to help identify the likely
211 causal mutations in the selected CoV-VIP genes. There is good evidence that the majority of
212 adaptive mutations in the human genome are regulatory mutations (Enard et al., 2014;
213 Kudaravalli et al., 2009; Nédélec et al., 2016; Quach et al., 2016) and, accordingly, we find that
214 iSAFE peaks are significantly closer to GTEx eQTLs proximal to CoV-VIP genes than expected
215 by chance (iSAFE peak proximity test, $P<10^{-9}$; Methods). Therefore, for each CoV-VIP gene, we
216 choose a variant with the lowest Relate p-value ($<10^{-3}$; Methods) that is situated at or close to a
217 GTEx eQTL associated with the focal gene to estimate the likely starting time of selection for
218 that gene (Methods; Figure S5).

219 Using this approach, we observe 42 CoV-VIPs (Table S5 and Figure S5) with selection starting
220 times clustered around a peak 870 generations ago (~200 generations wide, potentially due to
221 noise in our estimates; Figure 2). While this amounts to about four times more selected CoV-
222 VIP genes than were detected using either nSL or iHS (both detected around ten CoV-VIPs
223 amongst the top 200 ranked genes; Table S4) this is not unexpected as Relate has more power
224 to detect selection events than nSL and iHS when the beneficial allele is at intermediate
225 frequencies at the point of measurement (typically <60%; Figure 3; Enard and Petrov, 2020;
226 Ferrer-Admetlla et al., 2014; Voight et al., 2006). The relatively tight temporal clustering of
227 starting times forms a highly significant peak (peak significance test $P=2.3.10^{-4}$; Figure 2) when

228 comparing the observed clustering of CoV-VIPs start times with the distribution of inferred start
229 times for randomly sampled sets of genes (Methods). Note that this peak significance test is
230 gene clustering-aware (Methods). Further, this significance test is not biased by the fact that
231 CoV-VIPs are enriched for sweep signals, as the test remains highly significant ($P=1.10^{-4}$) when
232 using random control sets with comparable high-scoring nSL statistics (Methods). This suggests
233 that the tight temporal clustering of selection events is a specific feature of the CoV-VIPs, rather
234 than a confounding aspect of any gene set similarly enriched for sweeps.

235

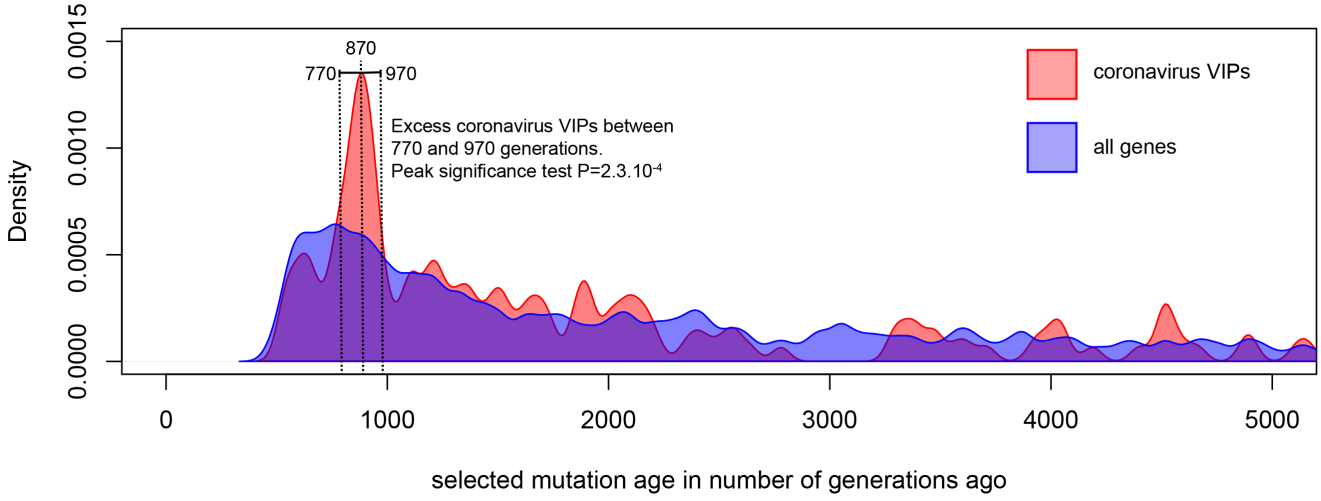

236

237 **Figure 2. Timing of selection at CoV-VIPs**
238 The figure shows the distribution of selection start times at CoV-VIPs (pink distribution)
239 compared to the distribution of selection start times at all loci in the genome (blue distribution).
240 Details on how the two distributions are compared by the peak significance test, and how the
241 selection start times are estimated with Relate, are provided in Methods.

242 The genes with clustered selection starting times around 900 generations ago are enriched in
243 strong nSL signals, as shown by running the peak significance test using only CoV-VIPs and
244 controls with strong nSL signals (Figure S6). Conversely, the peak disappears when restricting
245 this test to weaker nSL signals (P=0.53 when using the lowest 50% of nSL statistics; Methods).
246 Importantly, our estimates of the timing of selection are not biased by our use of methods that
247 rely on selected variants not being fixed in the population at the time of genome sampling (i.e.
248 Relate). When rerunning our analytical pipeline focusing only on strong candidate loci according
249 to Tajima's D (Tajima, 1989), a statistic developed to detect recently completed sweeps (i.e.
250 fixed mutations), we observe the same clustering of selection events starting around 900
251 generations ago (Figure S7). Further, the remaining 382 CoV-VIPs that are not part of this

252 temporal cluster around 900 generations ago are not more likely to have significant Tajima's D
253 values than controls (whole enrichment curve P=0.07). Consequently, our results are consistent
254 with the emergence of a viral epidemic ~900 generations, or ~25,000 years (900 generations *
255 28 years per generation; Moorjani et al., 2016), ago that drove a burst of strong positive
256 selection in the ancestors of East Asians, which may represent a genetic record of a multi-
257 generational viral epidemic amongst the 26 human populations tested here.

258 Although selective pressures other than a coronavirus or another unknown type of virus with
259 similar host interactions might also contribute to these patterns, we note that the signal is
260 restricted specifically at CoV-VIPs and none of 17 other viruses that we tested exhibit the same
261 temporal clustering ~900 generations ago in East Asia (peak significance test P>0.05 in all
262 cases; Methods). Further, this test remained highly significant when retesting the temporal
263 clustering of CoV-VIPs using only other RNA VIPs as the control set ($P=4.10^{-4}$; Table S1),
264 consistent with the clustered selection signals being a coordinated adaptive response to a
265 coronavirus or another virus using similar host interactions.

266

267 **Strong selection drove coordinated changes in multiple CoV-VIP genes over 20,000 years**

268 To learn more about the likely start and duration of the selection pressure acting on the
269 ancestors of East Asians, we use CLUES (Stern et al., 2019) to infer allele frequency
270 trajectories and selection coefficients for the inferred beneficial mutations proximal to the 42
271 CoV-VIP genes with selection starting 900 generations ago according to Relate (Figure 3).
272 CLUES uses the temporal variation in population size and coalescence rates inferred by Relate
273 to reconstruct frequency trajectories while taking demographic fluctuations into account. Our
274 observation of sweep signals at 42 CoV-VIP genes in the ancestors of East Asians suggests
275 that the putative underlying viral epidemic likely spanned many generations (i.e. the time
276 needed for selection to drive initially rare alleles to intermediate/high frequencies). Accordingly,
277 we anticipate that selection was probably strongest when the naive host population was first
278 infected by the virus, before gradually waning as the host population adapted to the viral
279 pressure (Hayward and Sella, 2019). Similarly, a decrease in the virulence of the virus over
280 time, a phenomenon that has been reported during the long term bouts of host-virus coevolution
281 (Best and Kerr, 2000), would also result in the gradual decrement of selection coefficients
282 across time. Hence, for each of the 42 CoV-VIPs predicted to have started coming under
283 selection ~900 generations ago, we use CLUES to estimate the selection coefficient in two

284 successive time-intervals (between 1,000 and 500 generations ago, and from 500 generations
285 ago to the present), predicting that selection would be stronger in the oldest interval. We note
286 that a 500 generations interval was reported as the approximate timespan that CLUES provides
287 reliable estimates for humans (Stern et al., 2019); using smaller generations intervals, we would
288 run the risk of getting overly noisy selection coefficient estimates based on too few coalescent
289 events. However, 500 generations intervals are not adequate to obtain reasonable estimates of
290 the precise duration of the selective pressure (Stern et al., 2019), so we do not attempt to
291 estimate this parameter here, and we simply try to compare the two time periods with each
292 other. Also, because CLUES uses a computationally intensive algorithm when following the
293 recommendations of Stern et al. (2020), we base our estimates on only two of the five East
294 Asian populations (i.e. Dai and Beijing Han Chinese; Figure 3A, B and 3C, D, respectively).

295 CLUES infers frequency trajectories that are more complex than a simple, clear, abrupt jump in
296 frequency 900 generations ago. Instead, the estimated frequency trajectories (Figure 3A,B,C,D)
297 suggest that 900 generations ago is the approximate time when the bulk of the selected variants
298 reached a frequency of a few percent or more, and approximately when there is an acceleration
299 in the frequency increase (Figure 3B, D). This might correspond to the transition between the
300 establishment and exponential phases of the sweeps, and might imply that the selective
301 pressure is older than 900 generations. The initially flatter, slower increases in frequency,
302 lasting sometimes up to 600 generations ago for some variants, are compatible with either co-
303 dominant or recessive alleles, and likely exclude dominant alleles that would start increasing in
304 frequency more abruptly. Interestingly, this would be in good agreement with the rarity of
305 dominant eQTLs in GTEx, if selected variants were indeed regulatory (GTEx Project, 2017).
306 Although the flat, slow starts of frequency increases make it hard to pinpoint when selection
307 started exactly, the vast majority of the selected alleles appear to have reached 5% or higher
308 frequencies by 600 generations, thus making it highly unlikely that the selective pressure would
309 have started 600 or less generations ago. Frequency trajectories estimated in the Yoruba
310 African population (Figure 4A) or the British European population (Figure 4B) also show very
311 low frequencies 900 generations ago. The selected variants in East Asia are found nowadays at
312 very low frequencies especially in Africa (Table S6). This implies that they are substantially
313 older than when selection started in East Asia, which may then be described as selection on low
314 frequency standing variation. Intriguingly, some variants rise in frequency (up to 40% frequency
315 at most) in Europe mostly after 800 generations ago. A small number of variants in Africa
316 increase in frequency (up to 30% frequency at most) after 600 generations ago.

317 The selected mutations are estimated to have continually increased in frequency in East Asia
318 until ~200 generations (approximately 5,000 years) ago, after which they remained relatively
319 stable (Figure 3A, C). Accordingly, CLUES estimates very high selection coefficients in the
320 interval between 1,000 and 500 generations ago (Dai average s = 0.034, Beijing Han average s
321 = 0.042; Figure 5A, B), but much weaker selection coefficients from 500 generations ago up to
322 the present (Dai average s = 0.002, Beijing Han average s = 0.003; Figure 5A, B). These
323 patterns are consistent with the appearance of a strong selective pressure that triggered a
324 coordinated adaptive response across multiple independent loci, which waned through time as
325 the host population adapted to the viral pressure and/or as the virus became less virulent.

326

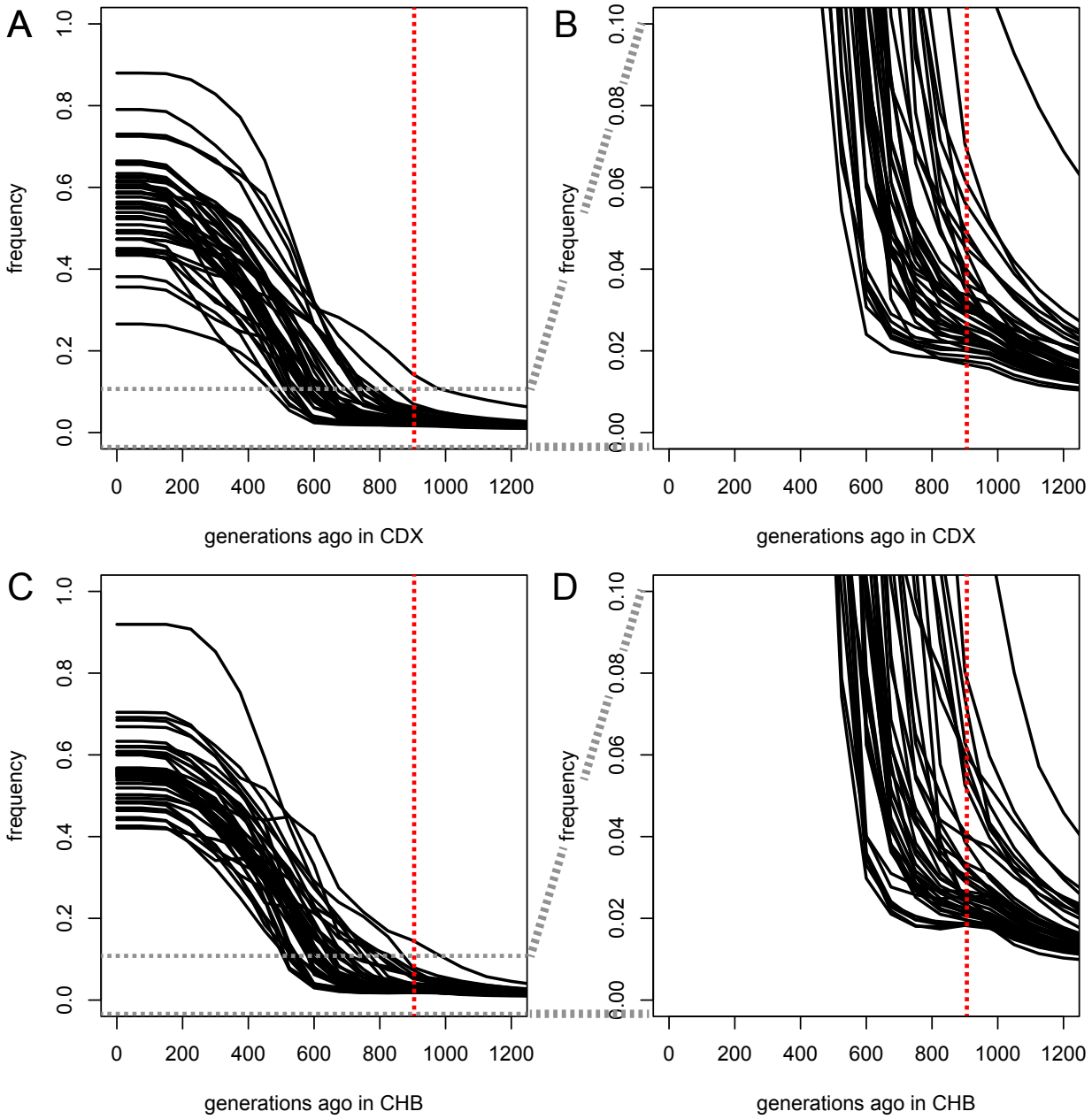

Figure 3. Selected CoV-VIPs allele frequency trajectories over time estimated by CLUES in East Asia

Each frequency trajectory is for one of the 42 Relate selected mutations at CoV-VIPs within the peak around 900 generations ago (Methods). A) Frequency trajectories in the Chinese Dai CDX 1,000 Genomes population. B) Same, but zoomed-in from frequencies 0 to 10%. C) Frequency trajectories in the Han Chinese from Beijing CHB 1,000 Genomes population. D) Same, but zoomed-in from frequencies 0 to 10%.

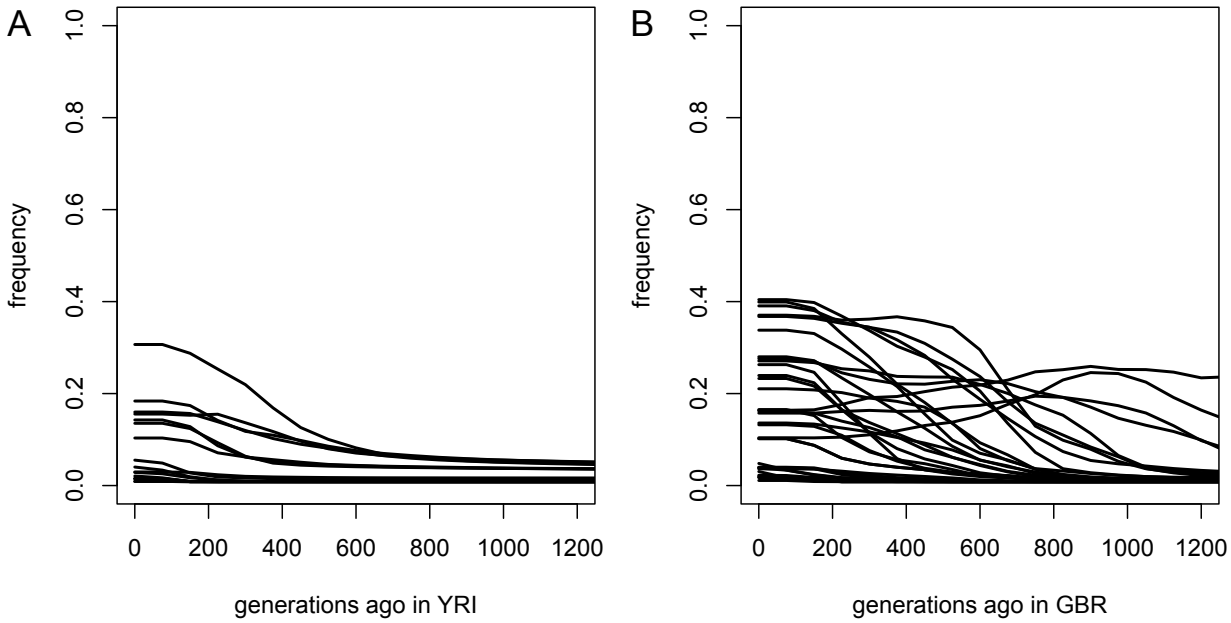

Figure 4. Selected CoV-VIPs allele frequency trajectories over time estimated by CLUES in Africa (Yoruba) and Europe (British)

Same as Figure 3. A) Yoruba population. The graph includes 17 frequency trajectories, the 25 other alleles selected in East Asia being absent in the Yoruba sample (but not Africa overall, see Table Sx) B) British population. The graph includes 35 frequency trajectories, the other seven alleles selected in East Asia being absent in the British sample.

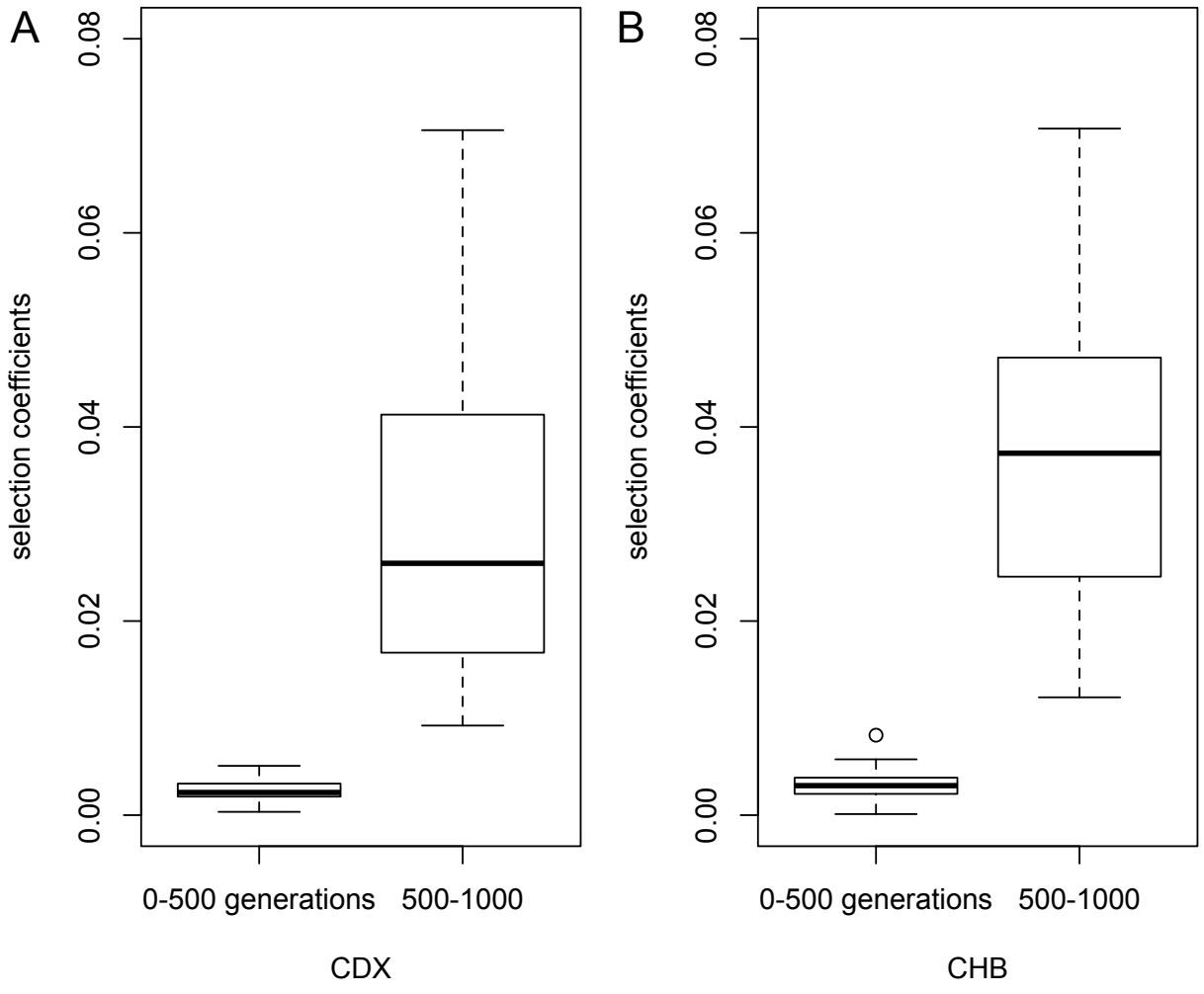

Figure 5. Coronavirus selected VIPs selection coefficients estimated by CLUES
This figure shows classic R boxplots of selected coefficients at the 42 Relate selected mutations within the peak around 900 generations ago (Methods). A) Selection coefficients in the Chinese Dai CDX 1,000 Genomes population. B) Selection coefficients in the Han Chinese from Beijing CHB 1,000 Genomes population. Left: average selection coefficients between 0 and 500 generations ago. Right: average selection coefficients between 500 and 1,000 generations ago.

Selected CoV-VIPs are enriched for antiviral and proviral factors

To further clarify that an ancient viral epidemic caused the strong burst of selection we observe in the ancestors of East Asians, and not another ecological pressure acting on the same set of genes, we test if the 42 selected CoV-VIPs are enriched for genes with antiviral or proviral effects relative to other CoV-VIPs (i.e. loci that are known to have a detrimental or beneficial effect on the virus, respectively). Because the relevant literature for coronaviruses is currently limited – which also applies to the relatively recent SARS-CoV-2 virus – we extend our set of

359 anti- and proviral loci beyond those associated with coronaviruses to include loci reported for
360 diverse viruses with high confidence from the general virology literature (see SI: *Host adaptation*
361 *is expected at VIPs*; Table S1). We find that 21 (50%) of the 42 CoV-VIPs that came under
362 selection ~900 generations ago have high-confidence anti- or proviral effects (vs. 29% for all
363 420 CoV-VIPs), a significant inflation in anti- and proviral effects (hypergeometric test $P=6.10^{-4}$)
364 that further supports our claim that the underlying selective pressure was most likely a viral
365 epidemic. This overlap of antiviral and proviral effects between different viruses also implies that
366 an unknown virus that happened to use similar VIPs as coronaviruses could have indeed been
367 responsible.

368 **Selected mutations lie near regulatory variants active in SARS-CoV-2 affected tissues**

369 Coronavirus infections in humans are known to have pathological consequences for specific
370 bodily tissues, whereby we investigate if the genes targeted by selection in the ancestors of
371 East Asians are also enriched for regulatory functions in similar tissues. In light of our finding
372 that many putative causal mutations in CoV-VIPs were proximal to eQTLs, we investigate
373 whether selected mutations are situated closer to eQTLs for a given tissue than expected by
374 chance, as this would indicate that the tissue was negatively impacted by the virus (prompting
375 the adaptive response). Note that the GTEx eQTLs we use are not specific to a single tissue
376 (eQTLs are rarely so in general), and are shared between tissues. However, each tissue still
377 has its own specific combination of eQTLs, thus making the results at each tissue not
378 completely redundant. Briefly, we estimate a proximity-based metric that quantifies the distance
379 between the location of the causal mutation estimated by iSAFE and the tissue-specific eQTLs
380 for the 42 loci that likely started coming under selection ~900 generations ago, and compare
381 this to the same distances observed amongst randomly sampled sets of CoV-VIPs (Figure 6;
382 Methods).

383 Using this approach, we find that GTEx lung eQTLs lie closer to predicted causal mutations
384 amongst the 42 putative selected loci than for any other tissue ($P=3.10^{-5}$; Figure 6). Several
385 additional tissues known to be negatively affected by coronavirus – blood and arteries (Bao et
386 al., 2020; Grosse et al., 2020), adipose tissue (Michalakis and Ilias, 2020) and the digestive
387 tract (Elmunzer et al., 2020) – also exhibit closer proximities between putative causal loci and
388 tissue-specific eQTLs than expected by chance (Figure 6). Interestingly, the spleen shows no
389 tendency for eQTLs to lie closer to selected loci than expected around 900 generations ago
390 compared to other evolutionary times, perhaps because the spleen is replete with multiple types

of immune cells that might be more prone to more regular adaptation in response to diverse pathogens over time, and less prone to adaptive bursts restricted over time in response to a specific pathogen (Quintana-Murci, 2019). Note that tissues with more eQTLs tend to have more significant p-values. For example skeletal muscle has a lower proximity ratio than stomach but also a lower p-value due to the higher statistical power provided by more eQTLs. Our results indicate that the tissues impacted in the inferred viral epidemic in ancestors of East Asians match those pathologically affected by the SARS-CoV-2 infection in contemporary populations, providing further evidence that this ancient infection might have been a coronavirus or another type of virus that used similar host interactions.

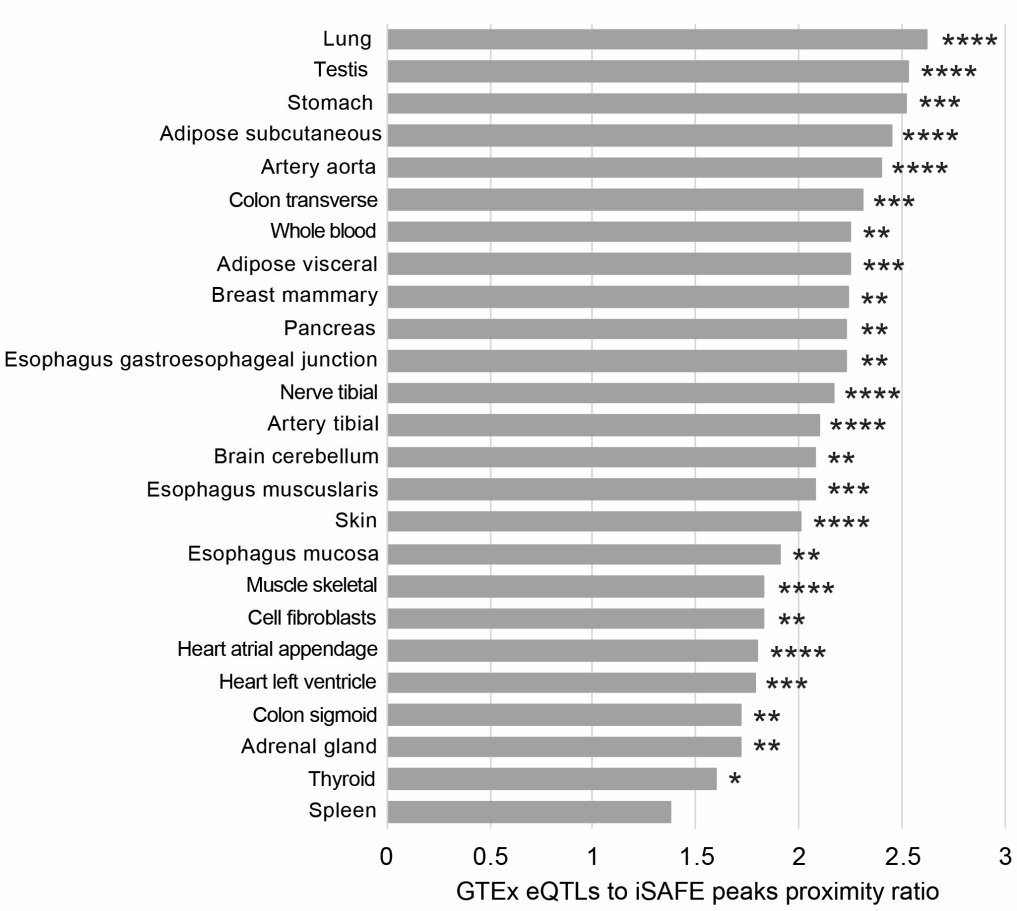

Figure 6. Proximity of selection signals to GTEx eQTLs at the 42 selected CoV-VIPs compared to random CoV-VIPs

The histogram shows how close selection signals localized by iSAFE peaks are to the GTEx eQTLs from 25 different tissues, at peak-VIPs compared to randomly chosen CoV-VIPs (Methods). How close iSAFE peaks are to GTEx eQTLs compared to random CoV-VIPs is estimated through a proximity ratio. The proximity ratio is described in the Methods. It quantifies how much closer iSAFE peaks are to eQTLs of a specific GTEx tissue, compared to random

408 expectations that take the number and structure of iSAFE peaks, as well as the number and
409 structure of GTEx eQTLs into account (Methods). Four stars: proximity ratio test P<0.0001.
410 Three stars: proximity ratio test P<0.001. Two stars: P<0.01. One star: P<0.05. Note that lower
411 proximity ratios can be associated with smaller p-values for tissues with more eQTLs (due to
412 decreased null variance; for example, skeletal muscle vs. pancreas).

413 **Coronavirus VIPs are enriched for SARS-CoV-2 susceptibility and COVID-19 severity loci**

414 Our results indicate that many of the selected CoV-VIPs now sit at intermediate to high
415 frequencies in modern East Asian populations. Accordingly, we anticipate that these
416 segregating loci should make a measurable contribution to the inter-individual variation in
417 SARS-CoV-2 susceptibility and (COVID-19) severity amongst contemporary populations in East
418 Asia, and predict that such loci would be readily detectable in a reasonably-powered genome
419 wide association study (GWAS) investigating these traits in East Asian populations. While such
420 a scan has yet to be reported for a large East Asian cohort, two GWASs were recently released
421 that used sizable British cohorts to investigate SARS-CoV-2 susceptibility (1,454 cases and
422 7,032 controls; henceforth called the susceptibility GWAS) and severity (325 cases [deaths]
423 versus 1,129 positive controls; henceforth called the severity GWAS) (data from the UK
424 Biobank; Sudlow et al., 2015; https://grasp.nhlbi.nih.gov/Covid19GWASResults.aspx). Because
425 we use a different population than the ones where we found selection, we only ask, as a form of
426 functional validation of a viral pressure, if there is an overlap between the selected loci in East
427 Asia and stronger COVID-19 GWAS hits in the UK Biobank cohort. We do not look at all at the
428 directionality or the size of effects, as it is dubious that those would be transposable between
429 populations. This also means that we make no claim at all here about any decrease or increase
430 of virus susceptibility in any given human population compared to others. Furthermore, we use
431 the UK-Biobank cohort instead of the complete COVID-19 Host Genetics Initiative meta-GWAS
432 data (https://www.covid19hg.org/; The COVID-19 Host Genetics Initiative, 2020), to avoid
433 population stratification to the best extent possible (a legitimate concern with a trait clearly
434 affected by environmental factors).

435 While we are unable to precisely identify the causal variants for the selected CoV-VIP genes
436 observed in the ancestors of East Asians – nor would these variants necessarily occur as
437 outliers in a GWAS conducted on the British population – we note that it is possible that other
438 variants in the same CoV-VIP genes may also produce variation in SARS-CoV-2 susceptibility
439 and severity amongst modern British individuals.

440 By contrasting variants in CoV-VIPs against those in random sets of genes, we find that variants
441 in CoV-VIPs have significantly lower p-values for both the susceptibility GWAS and severity
442 GWAS than expected (simple permutation test $P<10^{-9}$ for both GWAS tests; Methods). More
443 importantly, the 42 CoV-VIPs from the selection event starting ~900 generations ago have even
444 lower GWAS p-values compared to other CoV-VIPs (P=0.0015 for susceptibility GWAS and
445 P=0.023 for severity GWAS; Methods). This result indicates that the selected genes inferred in
446 our study might contribute to individual variation in COVID-19 etiology in modern human
447 populations in the UK, providing further evidence that a coronavirus or another virus with similar
448 host interactions may have been the selection pressure behind the adaptive response we
449 observe in the ancestors of East Asians. Notably, the strongest GWAS hits identified by the
450 COVID-19 Host Genetics Initiative (listed at https://www.covid19hg.org/publications/) do not
451 overlap with the 42 CoV-VIPs selected in East Asia. We note however that we do not
452 necessarily expect the strongest GWAS hits in Europe to be strong hits in other populations. In
453 addition, although adaptation implies a functional genetic effect, a genetic effect does not
454 necessarily mean it has adaptive potential. The lack of overlap with the strongest COVID-19
455 Host Genetics Initiative hits is therefore not necessarily very surprising. It also does not take
456 away the fact that we found an enrichment in stronger GWAS hits on average at CoV-VIPs and
457 especially at selected CoV-VIPs.

458 **Selected CoV-VIP genes include multiple known drug targets**

459 Our analyses suggest that the 42 CoV-VIPs identified as putative targets of an ancient
460 coronavirus (or another virus using similar host interactions) epidemic might play a functional
461 role in SARS-CoV-2 etiology in modern human populations. We find that four of these genes
462 (*SMAD3*, *IMPDH2*, *PPIB*, *GPX1*) are targets of eleven drugs being currently used or
463 investigated in clinical trials to mitigate COVID-19 symptoms (Methods). While this number is
464 not higher than expected when compared to other CoV-VIPs (hypergeometric test P>0.05), we
465 note that most of the 42 genes identified here have yet to be the focus of clinical trials for SARS-
466 CoV-2-related drugs. In addition to the four selected CoV-VIP genes targeted by coronavirus-
467 specific drugs, five additional selected CoV-VIPs are targeted by multiple drugs to treat a variety
468 of non-coronavirus pathologies (Table S7). This raises the possibility that such drugs could be
469 repurposed for therapeutic use in the current SARS-CoV-2 pandemic. Indeed, an additional six
470 of the 42 selected CoV-VIPs have been identified by (Finan et al., 2017) as part of the
471 “druggable genome” (Table S7).

472 # Discussion

473 By scanning 26 diverse human populations from five continental regions for evidence of strong
474 selection acting on genes that interact with coronavirus strains (CoV-VIPs), we identified a set of
475 42 CoV-VIPs exhibiting a coordinated adaptive response that likely emerged more than 20,000
476 years ago (Figure 2). This pattern was unique to the ancestors of East Asian populations (as
477 classified by the 1,000 Genomes, including South East Asia with the Kinh in Vietnam), being
478 absent from any of the 21 non East-Asian human populations tested here. By using ARG
479 methods to reconstruct the trajectories of selected alleles, we show that this selection pressure
480 produced a strong response across the 42 CoV-VIP genes that gradually waned and resulted in
481 the selected loci plateauing at intermediate frequencies. Further, we demonstrate that this
482 adaptive response is likely the outcome of a multigenerational viral epidemic, as attested by the
483 clustering of putatively selected loci around variants that regulate tissues known to exhibit
484 COVID-19-related pathologies, and the enrichment of variants associated with SARS-CoV-2
485 susceptibility and severity, as well as anti- and proviral functions, amongst the 42 CoV-VIP
486 genes selected starting around 900 generations ago.

487 An important limitation of our study is that some of our analyses rely upon comparative datasets
488 that were generated in contemporary human populations that have different ancestries than the
489 East Asian populations where the selected CoV-VIP genes were detected. In particular, both of
490 the eQTL and GWAS datasets come from large studies that are primarily focused on
491 contemporary populations from Europe, and none of the five European populations in our study
492 exhibit the selection signals observed in the genomes of East Asians. Accordingly, more direct
493 confirmation of the causal role of 42 CoV-VIP genes in COVID-19 etiology will require the
494 appropriate GWAS to be conducted in East Asian populations. The detection of genetic
495 associations amongst the 42 CoV-VIPs in a GWAS on contemporary East Asians would provide
496 further evidence that one or more coronaviruses, or another virus using similar interactions,
497 comprised the selection pressure that drove the observed adaptive response. Moreover, a high-
498 powered GWAS in East Asian populations would be required to identify the loci that currently
499 impact individual variation in COVID-19 etiology in East Asian individuals. Because of these
500 limitations, and because it would be extremely difficult to control for all the other factors that
501 differ across the world (including socioeconomic factors), our results do not represent evidence
502 for any difference in either increased or decreased genetic susceptibility in any human
503 population.

504 **Insights into ancient viral epidemics from modern human genomes**

505 A particularly salient feature of the adaptive response observed for the 42 CoV-VIPs is that
506 selection appears to be acting continuously over a ~20,000 years period, with the caveat that
507 the start of selection is complex to pinpoint as shown by the analysis of the selected alleles
508 frequency trajectories (Figure 3). The activity of a viral pressure over such an extensive time
509 period is not consistent with epidemics that started in recorded human history, which tend to be
510 circumscribed to a few generations. A possible hypothesis is that the viral pressure remained
511 present throughout the 20,000 year period, but was only initially strong enough to qualify as a
512 full-blown pandemic in the commonly understood sense, before becoming less severe over time
513 as a consequence of host adaptation and/or a reduction in virulence. As this manuscript was in
514 the final stages of preparation, the first host-virus interactomes were published for SARS-CoV-1
515 and MERS-CoV, which exhibit an extensive overlap with the SARS-CoV-2 interactome used in
516 the present study (Gordon et al., 2020). This suggests that coronaviruses share a broad set of
517 host proteins that they interact with, which should also apply to ancient coronaviruses. These
518 patterns are consistent with one or more coronaviruses driving selection events in East Asian
519 prehistory that produced the signals that we report here. That said, and as already mentioned,
520 we cannot exclude that another, currently unknown type of viruses might have been
521 responsible, that used the same interactions as coronaviruses with human proteins. The
522 cumulated evidence in this study still clearly points towards an ancient viral selective pressure.

523 Further validation of the historical trajectories of the causal mutations at selected genes is still
524 needed, including more finely resolved temporal and geographic patterns that could be derived
525 from ancient DNA sampled from across East Asia that span the human occupation of this
526 region; however, the requisite ancient samples are lacking at the moment. Nonetheless, we
527 note the geographic origin of several modern outbreaks of coronaviruses in East Asia, point to
528 East Asia being a likely location where these ancient populations came into contact with the
529 virus. Given that multiple recently recorded coronavirus outbreaks have been traced to
530 zoonoses (direct or indirect with other animal intermediates) from East Asian bats (Wong et al.,
531 2019), our results suggest that East Asia might have also been a natural range for coronavirus
532 reservoir species during the last 25,000 years.

533 **Applied evolutionary medicine: using evolutionary information to combat COVID-19**

534 The net result of the ancient selection patterns on the CoV-VIPs in ancient human populations is
535 the creation of genetic differences amongst individuals now living in East Asia, and between

536 East Asians and populations distributed across the rest of the world. As we demonstrate in this
537 study, this evolutionary genetic information can be exploited by statistical analyses to identify
538 loci that are potentially involved in the epidemiology of modern diseases – COVID-19 in the
539 present case. Such evolutionary information may ultimately assist in the development of future
540 drugs and therapies, by complementing information obtained from more traditional
541 epidemiological and biomedical research. For example, a recent study focusing on *TMPRSS2* –
542 a gene encoding for a transmembrane protein that plays a key role in SARS-CoV-2 infection –
543 found that East Asian populations carry two protein coding variant that are correlated with low
544 fatality rate for COVID-19 cases (Jeon et al., 2020). While such studies provide high quality
545 information on a specific gene, the evolutionary approach adopted here is able to leverage
546 evolutionary information embedded in modern genomes to identify candidate genomic regions
547 of interest. This is similar to the information provided by GWAS – i.e. lists of variants or genes
548 that are potentially associated with a particular trait or disease – though we note that the
549 information provided by evolutionary analyses comes with an added understanding about the
550 historical processes that created the underlying population genetic patterns.

551 The current limitation shared by population genomic approaches such as GWAS and the
552 evolutionary analyses presented here, is that they identify statistical associations, rather than
553 causal links, between genomic regions and traits, thereby necessitating additional research to
554 confirm causality. In addition to the various forms of empirical information that we provide here,
555 further evidence of causal relationships between the CoV-VIPs and COVID-19 etiology could be
556 obtained by examining which viral proteins the selected CoV-VIPs interact with, thus
557 establishing the specific viral functions that are affected. As a preliminary observation, we find
558 that the 35 of the 42 selected SARS-CoV-2 VIPs tend to interact with more viral proteins than
559 expected by chance (13 instead of six expected, see SI). Such information will help establish
560 genetic causality and will also improve our understanding of how hosts adapt in response to
561 viruses.

562 The ultimate confirmation of causality requires functional validation that the genes interact with
563 the virus, or that drugs targeting these genes have a knock-on impact for the virus. Notably,
564 several CoV-VIP genes are existing drug targets showing the functional importance of these
565 particular loci (Table S7), several of which are currently being investigated or used to treat
566 severe cases in the current COVID-19 pandemic. It remains to be established if the other genes
567 we have identified in this study might also help guide drug repurposing efforts and provide a
568 basis for future drug and therapeutic development to combat COVID-19 and related

569 pathologies. It also remains to be established if population-specific past adaptation, and the
570 underlying selected changes at those genes, could imply different drug efficacies in different
571 human populations.

572 Conclusion

573 By leveraging the evolutionary information contained in publicly available human genomic
574 datasets, we were able to infer ancient viral epidemics impacting the ancestors of contemporary
575 East Asian populations, which initially arose likely more than 20,000 years ago, resulting in
576 coordinated adaptive changes across 42 genes. Importantly, our evolutionary genomic analyses
577 have identified several new candidate genes that might benefit current efforts to combat COVID-
578 19, either by providing novel drug targets or by repurposing currently available drugs that target
579 these candidate genes (Tables S4 & S6). More broadly, our findings highlight the utility of
580 thinking about the possible contribution of evolutionary genomic approaches into standard
581 medical research protocols. Indeed, by revealing the identity of our ancient pathogenic foes,
582 evolutionary genomic methods may ultimately improve our ability to predict – and thus prevent –
583 the epidemics of the future.

584

585

586

587
588

589 # Methods

590 **Important note: for convenience, the 42 CoV-VIPs that we infer to have started coming**
591 **under selection around 900 generations ago are called peak-VIPs in the Methods.**

592 **Key resources table**

593

REAGENT or RESOURCE	SOURCE	IDENTIFIER
Deposited Data		
1000 Genome Project - Phase 3	(1000 Genomes Project Consortium, 2015)	ftp://ftp.1000genomes.ebi.ac.uk/vol1/ftp/release/20130502/
VIPs	–this manuscript	–Table S1
Relate-estimated coalescence rates, allele ages and selection P-values for the 1000GP	(Speidel et al., 2019)	https://zenodo.org/record/3234689
GTEx expression	(GTEx Project, 2017)	https://gtexportal.org/home/datasets
Protein-protein interactions (IntAct)	(Luisi et al., 2015)	https://www.ebi.ac.uk/intact
The density of conserved segments (PhastCons)	(Siepel et al., 2005)	http://hgdownload.cse.ucsc.edu/goldenPath/hg19/phastCons46way/
The density of regulatory elements	–	http://hgdownload.soe.ucsc.edu/goldenPath/hg19/encodeDCC/wgEncodeRegDnaseClustered
The recombination rate	(Hinch et al., 2011)	https://www.well.ox.ac.uk/~anjali/AAmap/
Software and Algorithms		

selscan (compute nSL).	(Szpiech and Hernandez, 2014)	https://github.com/szpiech/selscan
hapbin (compute iHS)	(Maclean et al., 2015)	https://github.com/evotools/hapbin
Gene Set Enrichment Pipeline	(Enard and Petrov, 2020)	https://github.com/DavidPierreEnard/Gene_Set_Enrichment_Pipeline
Relate	(Speidel et al., 2019)	https://myersgroup.github.io/relate/
CLUES	(Stern et al., 2019)	https://github.com/35ajstern/clues
iSAFE	(Akbari et al., 2018)	https://github.com/alek0991/iSAFE

Coronavirus VIPs

We used a dataset of 5,291 VIPs (Table S1). Of these, 1,920 of these VIPs are high confidence VIPs identified by low-throughput molecular methods, while the remaining VIPs were identified by diverse high-throughput mass-spectrometry studies. For a more detailed description of the VIPs dataset, please refer to SI: Host adaptation is expected at VIPs.

Genomes and sweeps summary statistics

To detect signatures of adaptation in various human populations, we used the 1,000 Genome Project phase 3 dataset which provides chromosome level phased data for 26 distinct human populations representing all major continental groups (1000 Genomes Project Consortium, 2015). To measure nSL separately in each of the 26 populations, we used the selscan software available at https://github.com/szpiech/selscan (Szpiech and Hernandez, 2014). To measure iHS, we used the hapbin software available at https://github.com/evotools/hapbin (Maclean et al., 2015).

608 **Ranking of sweep signals at protein-coding genes and varying window sizes**

609 To detect sweep enrichments at CoV-VIPs, we first order, separately in each of the 26 1,000
610 Genomes populations, human Ensembl (Cunningham et al., 2019) (version 83) protein-coding
611 genes according to the intensity of the sweep signals at each gene. As a proxy for the intensity
612 of these signals, we use the average of either iHS or nSL across all the SNPs with iHS or nSL
613 values within a window of fixed size, centered at the genomic center of genes, halfway between
614 the most upstream transcription start site and the most downstream transcription end site. We
615 then rank the genes according to the average iHS or nSL (more precisely their absolute values)
616 in these windows. We get six rankings for six different fixed window sizes: 50kb, 100kb, 200kb,
617 500kb, 1,000kb and 2,000kb. We do this to account for the variable size of sweeps of different
618 strengths. We then estimate the sweep enrichment at CoV-VIPs compared to controls over all
619 these different window sizes considered together, or at specific sizes, as described below and in
620 Enard & Petrov (Enard and Petrov, 2020).

621 **Estimating the whole ranking curve enrichment at CoV-VIPs and its statistical**
622 **significance**

623 To estimate a sweep enrichment in a set of genes, a typical approach is to use the outlier
624 approach to select, for example, the top 1% of genes with the most extreme signals. Here we
625 use a previously described approach to estimate a sweep enrichment while relaxing the
626 requirement to identify a single top set of genes. Instead of, for example, only estimating an
627 enrichment in the top 100 genes with the strongest sweep signals, we estimate the enrichment
628 over a wide range of top X genes, where X is allowed to vary from the top 10,000 to the top 10
629 with many intermediate values. This creates an enrichment curve as in Figure 1. Figure 1 shows
630 the estimated relative fold enrichments at CoV-VIPs compared to controls, from the top 1,000 to
631 the top 10 nSL. The statistical significance of the whole enrichment curve can then be estimated
632 by using block-randomized genomes, as described in Enard & Petrov (Enard and Petrov, 2020).
633 In brief, block-randomized genomes make it possible to generate a large number of random
634 whole enrichment curves while maintaining the same level of clustering of genes in the same
635 candidate sweeps as in the real genome, which effectively controls for gene clustering.
636 Comparing the real whole enrichment curve to the random ones then makes it possible to
637 estimate an unbiased false-positive risk (also known as False Discovery Rate in the context of
638 multiple testing) for the observed whole enrichment curve at CoV-VIPs. A single false positive
639 risk can be estimated for not just one curve but by summing over multiple curves combined,
640 thus making it possible to estimate a single false positive risk over any arbitrary numbers of rank

641 thresholds, window sizes, summary statistics, and populations. For instance, we estimate the
642 false-positive enrichment risk of $P=2.10^{-4}$ at CoV-VIPs for rank threshold from the top 10,000 to
643 top 10, over six window sizes, for the five East Asian populations in the 1,000 Genomes data,
644 and for both nSL and iHS, all considered together at once. This makes our approach more
645 versatile and sensitive to selection signals ranging from a few very strong sweeps, to many,
646 more moderately polygenic hitchhiking signals. The entire pipeline to estimate false-positive
647 risks with block-randomized genomes is available at
648 https://github.com/DavidPierreEnard/Gene_Set_Enrichment_Pipeline (Enard and Petrov, 2020).

649 **Building sets of controls matching for confounding factors**

650 To estimate a sweep enrichment at CoV-VIPs, we compare CoV-VIPs with random control sets
651 of genes selected far enough (>500kb) from CoV-VIPs that they are unlikely to overlap the
652 same large sweeps. We do not compare CoV-VIPs with completely random sets of control
653 genes. Instead, we use a previously described bootstrap test to build random control sets of
654 genes that match CoV-VIPs for a number of potential confounding factors that might explain a
655 sweep enrichment, rather than interactions with viruses. The bootstrap test has been described
656 in detail (Enard and Petrov, 2020), and is available at
657 https://github.com/DavidPierreEnard/Gene_Set_Enrichment_Pipeline.

658 We include 11 different potential confounding factors in the bootstrap test:

659 - average GTEx expression in 53 GTEx V6 tissues.
660 - GTEx expression in lymphocytes.
661 - GTEx expression in testis.
662 - the number of protein-protein interactions from the Intact database, curated by Luisi et al.
663 (Luisi et al., 2015).
664 - the Ensembl (v83) coding sequence density in a 50kb window centered on each gene.
665 - the density of conserved segments identified by PhastCons (Siepel et al., 2005)
666 (http://hgdownload.cse.ucsc.edu/goldenPath/hg19/phastCons46way/).
667 - the density of regulatory elements, estimated by the density of Encode DNase I V3 Clusters
668 (http://hgdownload.soe.ucsc.edu/goldenPath/hg19/encodeDCC/wgEncodeRegDnaseClustered/)
669 in a 50kb window centered on each gene.
670 - the recombination rate in a 200kb window centered on each gene (Hinch et al., 2011).
671 - the GC content in a 50kb window centered on each gene.

672 - the number of bacteria each gene interacts with, according to the Intact database (as of June
673 2019; https://www.ebi.ac.uk/intact/).
674 - the proportion of genes that are immune genes according to Gene Ontology annotations
675 GO:0006952 (defense response), GO:0006955 (immune response), and GO:0002376 (immune
676 system process) as of May 2020.

677 **Estimating adaptation start times at specific genes with Relate**

678 As times of emergence of adaptive mutations, we use the publicly available estimates from
679 Relate (https://myersgroup.github.io/relate/). Relate estimates mutation emergence times while
680 controlling for fluctuations of population size over time, based on the coalescence rates it
681 reconstructs after inferring ancestral recombination graphs at the scale of the whole genome
682 (Speidel et al., 2019). Relate provides two times of emergence of mutations, one low estimate
683 (less generations ago), and one high estimate (more generations ago). The low time estimate
684 corresponds to the time when Relate estimates an elevated probability that the frequency of the
685 mutation is different from zero. The high time estimate corresponds to the time when Relate
686 estimates that the probability is not too small that the frequency of the mutation is different from
687 zero. For our purpose of estimating when selection started, the low time estimate is the best
688 suited, because it provides an estimate of when the frequency of a selected mutation was
689 already high enough to distinguish from zero, for those mutations where selection started from a
690 very low frequency. For cases where selection started with standing genetic variants that were
691 already distinguishable from zero, the Relate low time estimates for the emergence of mutations
692 do not provide a good proxy for when selection actually started. Thus, if we were able to
693 estimate when selection started for standing genetic variants, we might be able to observe an
694 even stronger peak than the one we see when just relying on those variants where selection
695 started from low frequencies.

696 Using the low Relate time estimates is also justified due to the fact that the sweep establishment
697 phase can take very variable amounts of time before the start of the sweep exponential phase.
698 During the establishment phase, selected alleles are still mostly governed by drift which makes
699 pinpointing the actual starting time of selection difficult. In this context, the low Relate time
700 estimates provide an estimate of the time when the selected alleles were no longer at very low
701 frequencies not statistically different from zero, and closer to entering the exponential phase,
702 which provides a more certain time estimate for when selection started for certain.

703 An important step is then to choose at each CoV-VIP locus, and all the other control loci, which
704 Relate mutation to use to get a single time estimate for each locus. Note that here we make an
705 assumption that each locus has experienced only one single adaptive event. Given our finding
706 that iSAFE peaks at CoV-VIPs are much closer to GTEx V8 eQTLs than expected by chance, it
707 is likely that the selected adaptive mutations are regulatory mutations at, or close to annotated
708 eQTLs for a specific gene. They are not necessarily exactly located at eQTLs, because current
709 eQTLs annotations may still be incomplete, and in our case we use eQTLs identified in GTEx
710 V8 using mostly European individuals, even though we analyse selection signals in East Asian
711 populations. Because of these limitations, we use the Relate estimated time at the mutation
712 where Relate estimates the lowest positive selection p-value within 50kb windows centered on
713 eQTLs. We also only consider variants with a minor allele frequency greater than 20%, given
714 the signals detected by iHS and nSL that only have some power to detect incomplete sweeps
715 above 20% frequencies (Ferrer-Admetlla et al., 2014; Voight et al., 2006). This also excludes a
716 potential risk of confounding by low frequency neutral or weakly deleterious variants, that can
717 show selection-like patterns when their only way to escape removal early on is through a
718 chance, rapid frequency increase that can look like selection. The Relate selection test is based
719 on faster than expected coalescence rates given the population size at any given time, and its
720 results are publicly available at https://myersgroup.github.io/relate/. Note that the mutation with
721 the lowest Relate p-value does not always overlap with an iSAFE peak (Figure S5), which is not
722 entirely surprising if the haplotype signals exploited by both Relate and iSAFE partly
723 deteriorated due to recombination since the time selection at CoV-VIPs was strong (Figures 3
724 and 5). Both of these methods are indeed designed to locate the selected variant right after, or
725 during, active selection.

726 Because we work with five different East Asian populations, we more specifically select the
727 variant with the lowest Relate selection test p-value on average across all the five East Asian
728 populations. Then, we also use the corresponding average low Relate mutation time estimate
729 across the five East Asian populations. We do not attempt to estimate the selection time and p-
730 value by considering all 1,000 Genomes East Asian individuals tested together by Relate,
731 because then the Relate selection test is at a greater risk of being confounded by population
732 structure. Finally, we only consider CoV-VIPs and other control genes with an average Relate
733 selection test p-value lower than 10^{-3}, to make sure that we indeed use estimated times at
734 selected variants.

735 **The peak significance test**

736 To test if the peak of Relate time estimates around 900 generations ago at CoV-VIPs (Figure 2)
737 is expected simply by chance or not, we designed a peak significance test. The test compares
738 the peak at CoV-VIPs, with the top peaks obtained when repeatedly randomly sampling sets of
739 genes. We first identify the most prominent peak at CoV-VIPs by visual inspection of the pink
740 distribution of Relate times for CoV-VIPs compared to the blue distribution of Relate times for all
741 protein-coding genes with an estimated Relate time (Figure 2). To build these distributions, top
742 Relate selected mutations shared between multiple neighboring genes (CoV-VIPs or controls)
743 are counted only once, to avoid a confounding effect of gene clustering (152 selected variants at
744 CoV-VIPs, 1771 selected variants for all protein coding genes). The peak around 900
745 generations ago (870 generations more exactly) spans approximately 200 generations, where
746 the pink distribution is clearly above the blue one. We then use a 200 generations-wide window,
747 sliding every generation from 0 to 6,000 generations to verify the peak more rigorously. Sliding
748 one generation after another, each time we count the difference between the number of Relate
749 selected variants at CoV-VIPs that fall in the sliding 200 generations window, and the number of
750 Relate selected variants at all other genes that are not CoV-VIPs, weighted by the percentage
751 of variants found at CoV-VIPs, to correct for the different size of the two sets of variants. Using
752 this sliding window approach, the top of the peak is found at 870 generations, with a difference
753 of 19.5 additional Relate selected variants between 770 and 970 (870 plus or minus 100) at
754 CoV-VIPs compared to the null expectation.

755 We then repeat the sliding of a 200 generations window to identify the maximum peak and
756 measure the same difference, but this time for random sets of Relate selected variants of the
757 same size (152 selected variants out of the 1,771 selected variants). To estimate p-values, we
758 then compare the actual observed difference with the distribution of differences generated with
759 one million random samples.

760 As mentioned in the Results, one potential issue is that we run the peak significance test after
761 we already know that CoV-VIPs are enriched for iHS and nSL top sweeps, and especially
762 enriched for nSL top sweeps. This enrichment may skew the null expectation for the distribution
763 of Relate times at CoV-VIPs. In other words, there is a risk that any set of genes with the same
764 sweep enrichment might exhibit the same peak as CoV-VIP. As a result, comparing CoV-VIPs
765 with randomly chosen non-CoV-VIPs may not be appropriate. To test this, we repeat the peak
766 significance test, but this time comparing the peak at CoV-VIPs with the peaks at random sets
767 of non-CoV-VIPs that we build to have the same distribution of nSL ranks as CoV-VIPs. To do

768 this, we define nSL bins between ranks 1 and the highest rank with a rank step of 100 between
769 each bin, and we count how many Relate selected variants fall in each bin (each gene has one
770 nSL rank and one Relate selected variant). To build the random set, we then fill each of the 100
771 bins with the same number of random non-CoV-VIPs, as long as their nSL rank falls within that
772 bin. We use the average nSL rank over the five East Asian populations, and the lower
773 population-averaged rank of either 1 Mb or 2Mb window sizes (where we observe the strongest
774 enrichment at CoV-VIPs, see Results). The results of the peak significance test are unchanged
775 when using the matching nSL distribution (peak significance test P=1.10-4 vs. P=2.3.10-4
776 without matching nSL distribution).

777 In further agreement with the fact that the sweep enrichment does not confound the peak
778 significance test, the peak at CoV-VIPs stands out more when repeating the peak significance
779 test using a smaller nSL top rank limit (Figure S6). In this case, we compare sets of CoV-VIPs
780 and sets of controls both enriched in stronger sweep signals. Thus, if stronger sweep signals at
781 CoV-VIPs biased the peak significance test, we would expect the peak to fade away when
782 comparing only CoV-VIPs and controls both with stronger nSL signals. Conversely, we observe
783 that half of the CoV-VIPs with the weaker nSL signals (population-averaged nSL rank higher
784 than 7,200 for both 1Mb and 2Mb windows) do not show a significant peak (peak significance
785 test P=0.53).

786 **The iSAFE peaks/eQTL proximity test**

787 Adaptation in the human genome was likely mostly regulatory adaptation through gene
788 expression changes (Enard et al., 2014; Kudaravalli et al., 2009; Nédélec et al., 2016; Quach et
789 al., 2016). To test if positive selection at CoV-VIPs likely involved regulatory changes, we ask
790 whether the signals of adaptation around CoV-VIPs are localized closer than expected by
791 chance to GTEx eQTLs that affect the expression of CoV-VIPs in present human populations.
792 Indeed, the genomic regions at or close to CoV-VIP GTEx eQTLs are likely enriched for CoV-
793 VIP regulatory elements, and therefore the most likely place to find CoV-VIP-related adaptations
794 in the genome. To localize where adaptation occurred, we use the iSAFE method that was
795 specifically designed for this purpose (Akbari et al., 2018). iSAFE scans the genome and
796 estimates a score that increases together with proximity to the actual selected mutation. The
797 higher the score, the higher the odds that the scored variant is itself the selected one, or close
798 to the selected one. An important caveat is that iSAFE is designed to localize where selection
799 happened right after it happened, or as selection is still ongoing. In our case, we have evidence

800 that selection was strong at CoV-VIPs only more than 500 generations (~14,000 years) ago,
801 and then much weaker more recently (Figure 5). This could be an issue, because we expect
802 that recombination events that occurred after the strong selection might have deteriorated the
803 iSAFE signal that relies on haplotype structure. This is because recombination mixes together
804 the haplotypes that hitchhiked with the selected mutation, with those that did not. In line with
805 this, we often do not observe simple, clean iSAFE score peaks, but instead, iSAFE score
806 plateaus and more rugged peaks (Figure S5). For this reason, we designed an approach to not
807 only identify the top of simple iSAFE peaks, but also more rugged peaks or plateaus. First, to
808 measure iSAFE scores, we combine all the haplotypes from the five East Asian populations
809 together as input, since we found that the selection signal at CoV-VIPs is common to all these
810 populations (iSAFE parameters: --IgnoreGaps --MaxRegionSize 250000000 --window 300 --
811 step 100 --MaxFreq .95 --MaxRank 15). We then use a 500kb window sliding every 10kb to
812 identify the highest local iSAFE value in the 500kb window (Figure S8). Once we have the
813 highest local iSAFE value and coordinate, we define a broader iSAFE peak as the region both
814 upstream and downstream where the iSAFE values are still within 80% of the maximum value
815 (Figure S8). This way, we can better annotate iSAFE plateaus and rugged peaks, and take into
816 account the fact that they can span more than just a narrow local maximum (Figure S5).

817 Once the local iSAFE peaks are identified, we can ask how close GTEx eQTLs are to these
818 peaks compared to random expectations. We first measure the distance of each CoV-VIP GTEx
819 eQTL to the closest iSAFE peak. To avoid redundancy, we merge eQTLs closer than 1kb to
820 each other into one test eQTL at the closest, lower multiple of 1,000 genomic coordinates (for
821 example 3,230 and 3,950 would both become 3,000). We then measure the average of the log
822 of the distance between all CoV-VIPs and their closest iSAFE peak. We use the log (base 10) of
823 the distance, because it matters if the eQTL/iSAFE peak distance is 100 bases instead of
824 200kb, but it does not really matter if the distance is 200kb or 600kb, because the iSAFE peak
825 at 300kb is likely not related to the eQTL more than the peak at 600kb. Once we have the
826 average of log-distances, we compare it to its random expected distribution. To get this random
827 distribution, we measure the log-distance between each CoV-VIP eQTL and the iSAFE peaks,
828 but after shifting the iSAFE scores left or right by a random value between 1Mb and 2Mb (Figure
829 S8; less, or no shift at all if this falls within telomeres or centromeres). We shift by at least 1Mb
830 to make sure that we do not rebuild the original overlap of iSAFE peaks with eQTLs again and
831 again (some iSAFE peaks, or more precisely rugged peaks and plateaus can be wide and
832 include several hundred kilobases; see Figure S5). The random shifting effectively breaks the

833 relationship between eQTLs and iSAFE peaks, while maintaining the same overall eQTL and
834 peak structure (and thus variance for the test). The random log-distance distribution then
835 provides an overall random average log-distance to compare the observed average long-
836 distance with, as well as estimate a p-value.

837 Then, to more specifically ask if lung eQTLs at CoV-VIPs or the eqTLs of other specific tissues
838 are closer to iSAFE peaks than expected by chance, we can do the same but only using the
839 eQTLs of that specific tissue. The analysis represented in figure 6 is however more complicated
840 than just testing if CoV-VIP eQTLs for a specific tissue are closer to iSAFE peaks than expected
841 by chance by randomly sliding iSAFE values. Instead, what we ask is whether the 42 peak-VIPs
842 have eQTLs for a given tissue that are even closer to iSAFE peaks than the eQTLs of all CoV-
843 VIPs in general. To test this, for example with lung eQTLs, we first estimate how close lung
844 eQTLs are to iSAFE peaks at peak-VIPs, compared to random expectations, by measuring the
845 difference between the observed and the average random log-distance, just as described
846 before. We then count the number of peak-VIPs with lung eQTLs (19 out of 25 peak-VIPs with
847 GTEx eQTLs), and we randomly select the same number of any CoV-VIP (which may randomly
848 include peak-VIPs) as long as the random set of CoV-VIPs has the same number of lung eQTLs
849 (plus or minus 10%) as the set of peak VIPs with lung eQTLs (the same gene can have multiple
850 eQTLs for one tissue). We make sure that the tested and the random sets have similar numbers
851 of genes and eQTLs so that the test has the appropriate null variance. We then measure the
852 difference between the observed log-distance, and the randomly expected average log-distance
853 for the random set of CoV-VIPs, exactly the same way we did before for the actual set of peak-
854 VIPs. We then measure the ratio of the observed difference in log-distance between peak-VIPs
855 and the random expectation after many random shiftings (1,000), divided by the average of the
856 same difference measured over many random sets of CoV-VIPs. The final ratio tells us how
857 much closer lung eQTLs are to iSAFE peaks at peak-VIPs compared to CoV-VIPs in general,
858 and still takes the specific eQTLs and iSAFE peak structures at each locus into account, since
859 we compare differences in log-distances expected while preserving the same eQTL and iSAFE
860 peak structure (see above the description of the random coordinate shifting). One important last
861 detail about the test is that because we already found that the 50% of loci with the lowest nSL
862 signals do not show a peak of selection at CoV-VIPs around 900 generations ago (see Results),
863 we do not use these loci in this test since any iSAFE peak there is much more likely to represent
864 random noise, not actual selection locations, and thus likely to dilute genuine signals. Using this
865 test, we find that lung and other tissues' eQTLs at peak-VIPs are much closer to iSAFE peaks

866 than they are at CoV-VIPs in general. This test thus specifically tells that adaptation happened
867 closer to lung eQTLs, specifically around 900 generations ago compared to other evolutionary
868 times. By estimating the same ratio for 24 other tissues with at least 10 peak-VIPs with the
869 specific tested tissue eQTLs, we can finally rank each tissue for its more pronounced
870 involvement in adaptation ~900 generations ago, as done in figure 6. It is particularly interesting
871 in this respect that the tissue with least evidence for being more involved in adaptation at that
872 time more than other evolutionary times is spleen. Spleen indeed likely represents a good
873 negative control as a tissue strongly enriched in immune cell types and likely to have evolved
874 adaptively for most of evolution.

875 **UK Biobank GWAS analysis**

876 To compare the UK Biobank GWAS p-values at different loci, we assigned one p-value for each
877 gene, either CoV-VIPs, peak-VIPs or other genes, even though each gene locus can have many
878 variants with associated GWAS p-values. To assign just one single GWAS p-value to each
879 gene, we selected the variant with the lowest p-value at or very close (<1kb) to GTEx eQTLs for
880 a specific gene, in line with the fact that GWAS hits tend to overlap eQTLs (Hormozdiari et al.,
881 2016), and to remain consistent with the rest of our manuscript. We then compared the average
882 p-value between different sets of genes using classic permutations (one billion iterations).

883 **Drug targets identification**

884 We queried the databases DGIdb (Cotto et al., 2017), and PanDrugs (Piñeiro-Yáñez et al.,
885 2018) for drugs targeting CoV-VIPs and peak-VIPs. For hits from PanDrugs we limited the
886 results to only genes that are in direct interaction with the designated drug. Drugs targeting
887 peak-VIPs are presented in Table S7. In addition, we present a list of peak-VIPs that are not
888 currently drug targets, but have been previously identified in (Finan et al., 2017) as viable drug
889 targets (druggable genome).

890 # Acknowledgments

891 We wish to thank Leo Speidel and Aaron Stern for their valuable help using Relate and CLUES,
892 respectively. Y.S. is supported by the Australian Research Council (ARC DP190103705). R.T. is
893 an ARC DECRA fellow (DE190101069).
894
895

Authors Contributions

Conceived and designed the experiments: YS, RT, DE. Performed the experiments: YS, MEL, RT, DE. Interpreted the results: YS, MEL, RT,CDH, ASJ, DE. Wrote the manuscript: YS, RT, DE

References

1000 Genomes Project Consortium (2015). A global reference for human genetic variation. Nature *526*, 68–74.

Akbari, A., Vitti, J.J., Iranmehr, A., Bakhtiari, M., Sabeti, P.C., Mirarab, S., and Bafna, V. (2018). Identifying the favored mutation in a positive selective sweep. Nat. Methods *15*, 279–282.

Balogun, O.D., Bea, V.J., and Phillips, E. (2020). Disparities in Cancer Outcomes Due to COVID-19—A Tale of 2 Cities. JAMA Oncol.

Bao, C., Tao, X., Cui, W., Yi, B., Pan, T., Young, K.H., and Qian, W. (2020). SARS-CoV-2 induced thrombocytopenia as an important biomarker significantly correlated with abnormal coagulation function, increased intravascular blood clot risk and mortality in COVID-19 patients. Exp. Hematol. Oncol. *9*, 16.

Barreiro, L.B., Ben-Ali, M., Quach, H., Laval, G., Patin, E., Pickrell, J.K., Bouchier, C., Tichit, M., Neyrolles, O., Gicquel, B., et al. (2009). Evolutionary dynamics of human Toll-like receptors and their different contributions to host defense. PLoS Genet. *5*, e1000562.

Best, S.M., and Kerr, P.J. (2000). Coevolution of host and virus: the pathogenesis of virulent and attenuated strains of myxoma virus in resistant and susceptible European rabbits. Virology *267*, 36–48.

Cotto, K.C., Wagner, A.H., Feng, Y.-Y., Kiwala, S., Coffman, A.C., Spies, G., Wollam, A., Spies, N.C., Griffith, O.L., and Griffith, M. (2017). DGIdb 3.0: a redesign and expansion of the drug–gene interaction database. Nucleic Acids Res. *46*, D1068–D1073.

Cunningham, F., Achuthan, P., Akanni, W., Allen, J., Amode, M.R., Armean, I.M., Bennett, R., Bhai, J., Billis, K., Boddu, S., et al. (2019). Ensembl 2019. Nucleic Acids Res. *47*, D745–D751.

Dong, E., Du, H., and Gardner, L. (2020). An interactive web-based dashboard to track COVID-19 in real time. Lancet Infect. Dis. *20*, 533–534.

eGTEx Project (2017). Enhancing GTEx by bridging the gaps between genotype, gene expression, and disease. Nat. Genet. *49*, 1664–1670.

Ellinghaus, D., Degenhardt, F., Bujanda, L., Buti, M., Albillos, A., Invernizzi, P., Fernández, J., Prati, D., Baselli, G., Asselta, R., et al. (2020). Genomewide Association Study of Severe Covid-19 with Respiratory Failure. N. Engl. J. Med.

Elmunzer, B.J., Spitzer, R.L., Foster, L.D., Merchant, A.A., Howard, E.F., Patel, V.A., West,

930 M.K., Qayed, E., Nustas, R., Zakaria, A., et al. (2020). Digestive Manifestations in Patients
931 Hospitalized with COVID-19. Clin. Gastroenterol. Hepatol.

932 Enard, D., and Petrov, D.A. (2018). Evidence that RNA Viruses Drove Adaptive Introgression
933 between Neanderthals and Modern Humans. Cell *175*, 360–371.e13.

934 Enard, D., and Petrov, D.A. (2020). Ancient RNA virus epidemics through the lens of recent
935 adaptation in human genomes. Philos. Trans. R. Soc. Lond. B Biol. Sci. *375*, 20190575.

936 Enard, D., Messer, P.W., and Petrov, D.A. (2014). Genome-wide signals of positive selection in
937 human evolution. Genome Res. *24*, 885–895.

938 Enard, D., Cai, L., Gwennap, C., and Petrov, D.A. (2016). Viruses are a dominant driver of
939 protein adaptation in mammals. Elife *5*, 56.

940 Ferrer-Admetlla, A., Liang, M., Korneliussen, T., and Nielsen, R. (2014). On detecting
941 incomplete soft or hard selective sweeps using haplotype structure. Mol. Biol. Evol. *31*, 1275–
942 1291.

943 Finan, C., Gaulton, A., Kruger, F.A., Lumbers, R.T., Shah, T., Engmann, J., Galver, L., Kelley,
944 R., Karlsson, A., Santos, R., et al. (2017). The druggable genome and support for target
945 identification and validation in drug development. Sci. Transl. Med. *9*.

946 Gene Ontology Consortium (2015). Gene Ontology Consortium: going forward. Nucleic Acids
947 Res. *43*, D1049–D1056.

948 Gordon, D.E., Jang, G.M., Bouhaddou, M., Xu, J., Obernier, K., White, K.M., O'Meara, M.J.,
949 Rezelj, V.V., Guo, J.Z., Swaney, D.L., et al. (2020). A SARS-CoV-2 protein interaction map
950 reveals targets for drug repurposing. Nature *583*, 459–468.

951 Grosse, C., Grosse, A., Salzer, H.J.F., Dünser, M.W., Motz, R., and Langer, R. (2020). Analysis
952 of cardiopulmonary findings in COVID-19 fatalities: High incidence of pulmonary artery thrombi
953 and acute suppurative bronchopneumonia. Cardiovasc. Pathol. *49*, 107263.

954 Hayward, L.K., and Sella, G. (2019). Polygenic adaptation after a sudden change in
955 environment.

956 Hinch, A.G., Tandon, A., Patterson, N., Song, Y., Rohland, N., Palmer, C.D., Chen, G.K., Wang,
957 K., Buxbaum, S.G., Akylbekova, E.L., et al. (2011). The landscape of recombination in African
958 Americans. Nature *476*, 170–175.

959 Hoffmann, C., and Kamps, B.S. (2003). SARS Reference (Flying Publisher).

960 Hormozdiari, F., van de Bunt, M., Segrè, A.V., Li, X., Joo, J.W.J., Bilow, M., Sul, J.H.,
961 Sankararaman, S., Pasaniuc, B., and Eskin, E. (2016). Colocalization of GWAS and eQTL
962 Signals Detects Target Genes. Am. J. Hum. Genet. *99*, 1245–1260.

963 Jeon, S., Blazyte, A., Yoon, C., Ryu, H., Jeon, Y., Bhak, Y., Bolser, D., Manica, A., Shin, E.-S.,
964 Cho, Y.S., et al. (2020). Ethnicity-dependent allele frequencies are correlated with COVID-19
965 case fatality rate (Authorea, Inc.).

966 Kudaravalli, S., Veyrieras, J.-B., Stranger, B.E., Dermitzakis, E.T., and Pritchard, J.K. (2009).
967 Gene expression levels are a target of recent natural selection in the human genome. Mol. Biol.

968 Evol. *26*, 649–658.

969 Luisi, P., Alvarez-Ponce, D., Pybus, M., Fares, M.A., Bertranpetit, J., and Laayouni, H. (2015).
970 Recent positive selection has acted on genes encoding proteins with more interactions within
971 the whole human interactome. Genome Biol. Evol. *7*, 1141–1154.

972 Maclean, C.A., Chue Hong, N.P., and Prendergast, J.G.D. (2015). hapbin: An Efficient Program
973 for Performing Haplotype-Based Scans for Positive Selection in Large Genomic Datasets. Mol.
974 Biol. Evol. *32*, 3027–3029.

975 Michalakis, K., and Ilias, I. (2020). SARS-CoV-2 infection and obesity: Common inflammatory
976 and metabolic aspects. Diabetes Metab. Syndr. *14*, 469–471.

977 Moorjani, P., Sankararaman, S., Fu, Q., Przeworski, M., Patterson, N., and Reich, D. (2016). A
978 genetic method for dating ancient genomes provides a direct estimate of human generation
979 interval in the last 45,000 years. Proc. Natl. Acad. Sci. U. S. A. *113*, 5652–5657.

980 Nédélec, Y., Sanz, J., Baharian, G., Szpiech, Z.A., Pacis, A., Dumaine, A., Grenier, J.-C.,
981 Freiman, A., Sams, A.J., Hebert, S., et al. (2016). Genetic Ancestry and Natural Selection Drive
982 Population Differences in Immune Responses to Pathogens. Cell *167*, 657–669.e21.

983 Ou, X., Liu, Y., Lei, X., Li, P., Mi, D., Ren, L., Guo, L., Guo, R., Chen, T., Hu, J., et al. (2020).
984 Characterization of spike glycoprotein of SARS-CoV-2 on virus entry and its immune cross-
985 reactivity with SARS-CoV. Nat. Commun. *11*, 1620.

986 Piñeiro-Yáñez, E., Reboiro-Jato, M., Gómez-López, G., Perales-Patón, J., Troulé, K.,
987 Rodríguez, J.M., Tejero, H., Shimamura, T., López-Casas, P.P., Carretero, J., et al. (2018).
988 PanDrugs: a novel method to prioritize anticancer drug treatments according to individual
989 genomic data. Genome Med. *10*, 41.

990 Quach, H., Rotival, M., Pothlichet, J., Loh, Y.-H.E., Dannemann, M., Zidane, N., Laval, G.,
991 Patin, E., Harmant, C., Lopez, M., et al. (2016). Genetic Adaptation and Neandertal Admixture
992 Shaped the Immune System of Human Populations. Cell *167*, 643–656.e17.

993 Quintana-Murci, L. (2019). Human Immunology through the Lens of Evolutionary Genetics. Cell
994 *177*, 184–199.

995 Richman, D.D., Whitley, R.J., and Hayden, F.G. (2020). Clinical Virology (John Wiley & Sons).

996 Roberts, G.H.L., Park, D.S., Coignet, M.V., McCurdy, S.R., Knight, S.C., Partha, R., Rhead, B.,
997 Zhang, M., Berkowitz, N., Baltzell, A.K.H., et al. (2020). AncestryDNA COVID-19 Host Genetic
998 Study Identifies Three Novel Loci. medRxiv.

999 Sabeti, P.C., Schaffner, S.F., Fry, B., Lohmueller, J., Varilly, P., Shamovsky, O., Palma, A.,
1000 Mikkelsen, T.S., Altshuler, D., and Lander, E.S. (2006). Positive natural selection in the human
1001 lineage. Science *312*, 1614–1620.

1002 Sattar Naveed, McInnes Iain B., and McMurray John J.V. (2020). Obesity Is a Risk Factor for
1003 Severe COVID-19 Infection. Circulation *142*, 4–6.

1004 Sawyer, S.L., Wu, L.I., Emerman, M., and Malik, H.S. (2005). Positive selection of primate
1005 TRIM5α identifies a critical species-specific retroviral restriction domain. Proc. Natl. Acad. Sci.
1006 U. S. A. *102*, 2832–2837.

1007 Scarpone, C., Brinkmann, S.T., Große, T., Sonnenwald, D., Fuchs, M., and Walker, B.B. (2020).
1008 A multimethod approach for county-scale geospatial analysis of emerging infectious diseases: a
1009 cross-sectional case study of COVID-19 incidence in Germany. Int. J. Health Geogr. *19*, 32.

1010 Schrider, D.R. (2020). Background Selection Does Not Mimic the Patterns of Genetic Diversity
1011 Produced by Selective Sweeps. Genetics *216*, 499–519.

1012 Siepel, A., Bejerano, G., Pedersen, J.S., Hinrichs, A.S., Hou, M., Rosenbloom, K., Clawson, H.,
1013 Spieth, J., Hillier, L.W., Richards, S., et al. (2005). Evolutionarily conserved elements in
1014 vertebrate, insect, worm, and yeast genomes. Genome Res. *15*, 1034–1050.

1015 Speidel, L., Forest, M., Shi, S., and Myers, S.R. (2019). A method for genome-wide genealogy
1016 estimation for thousands of samples. Nat. Genet. *51*, 1321–1329.

1017 Stern, A.J., Wilton, P.R., and Nielsen, R. (2019). An approximate full-likelihood method for
1018 inferring selection and allele frequency trajectories from DNA sequence data. PLoS Genet. *15*,
1019 e1008384.

1020 Stern, A.J., Speidel, L., Zaitlen, N.A., and Nielsen, R. (2020). Disentangling selection on
1021 genetically correlated polygenic traits using whole-genome genealogies. bioRxiv.

1022 Sudlow, C., Gallacher, J., Allen, N., Beral, V., Burton, P., Danesh, J., Downey, P., Elliott, P.,
1023 Green, J., Landray, M., et al. (2015). UK biobank: an open access resource for identifying the
1024 causes of a wide range of complex diseases of middle and old age. PLoS Med. *12*, e1001779.

1025 Szpiech, Z.A., and Hernandez, R.D. (2014). selscan: an efficient multithreaded program to
1026 perform EHH-based scans for positive selection. Mol. Biol. Evol. *31*, 2824–2827.

1027 Tajima, F. (1989). Statistical method for testing the neutral mutation hypothesis by DNA
1028 polymorphism. Genetics *123*, 585–595.

1029 The COVID-19 Host Genetics Initiative (2020). The COVID-19 Host Genetics Initiative, a global
1030 initiative to elucidate the role of host genetic factors in susceptibility and severity of the SARS-
1031 CoV-2 virus pandemic. Eur. J. Hum. Genet. *28*, 715–718.

1032 Uricchio, L.H., Petrov, D.A., and Enard, D. (2019). Exploiting selection at linked sites to infer the
1033 rate and strength of adaptation. Nat Ecol Evol *3*, 977–984.

1034 Voight, B.F., Kudaravalli, S., Wen, X., and Pritchard, J.K. (2006). A map of recent positive
1035 selection in the human genome. PLoS Biol. *4*, e72.

1036 Wong, A.C.P., Li, X., Lau, S.K.P., and Woo, P.C.Y. (2019). Global Epidemiology of Bat
1037 Coronaviruses. Viruses *11*.

1038 World Health Organization (2019). Middle East respiratory syndrome coronavirus (MERS-CoV).

1039 Zeberg, H., and Pääbo, S. (2020). The major genetic risk factor for severe COVID-19 is
1040 inherited from Neandertals.

1041